1-1-2016

Rapid emergence of life shown by discovery of 3,700-million-year-old microbial structures

Allen Phillip Nutman
University of Wollongong, University of New South Wales, anutman@uow.edu.au

Vickie C. Bennett
Australian National University, University of New South Wales, vickie.bennett@anu.edu.au

Clark R. L Friend
Glendale, UK, crlfriend@yahoo.co.uk

Martin J. Van Kranendonk
University of New South Wales, m.vankranendonk@unsw.edu.au

Allan Chivas
University of Wollongong, toschi@uow.edu.au

Rapid emergence of life shown by discovery of 3,700-million-year-old microbial structures

Abstract

Biological activity is a major factor in Earth's chemical cycles, including facilitating CO2 sequestration and providing climate feedbacks. Thus a key question in Earth's evolution is when did life arise and impact hydrosphere-atmosphere-lithosphere chemical cycles? Until now, evidence for the oldest life on Earth focused on debated stable isotopic signatures of 3,800-3,700 million year (Myr)-old metamorphosed sedimentary rocks and minerals1,2 from the Isua supracrustal belt (ISB), southwest Greenland3. Here we report evidence for ancient life from a newly exposed outcrop of 3,700-Myr-old metacarbonate rocks in the ISB that contain 1-4-cm-high stromatolites-macroscopically layered structures produced by microbial communities. The ISB stromatolites grew in a shallow marine environment, as indicated by seawater-like rare-earth element plus yttrium trace element signatures of the metacarbonates, and by interlayered detrital sedimentary rocks with cross-lamination and storm-wave generated breccias. The ISB stromatolites predate by 220 Myr the previous most convincing and generally accepted multidisciplinary evidence for oldest life remains in the 3,480-Myr-old Dresser Formation of the Pilbara Craton, Australia4,5. The presence of the ISB stromatolites demonstrates the establishment of shallow marine carbonate production with biotic CO2 sequestration by 3,700 million years ago (Ma), near the start of Earth's sedimentary record. A sophistication of life by 3,700 Ma is in accord with genetic molecular clock studies placing life's origin in the Hadean eon (>4,000 Ma)6.

Keywords

emergence, life, shown, discovery, rapid, 3, structures, 700, million, year, old, microbial

Disciplines

Medicine and Health Sciences | Social and Behavioral Sciences

Publication Details

Nutman, A. P., Bennett, V. C., Friend, C. R. L., Van Kranendonk, M. J. & Chivas, A. R. (2016). Rapid emergence of life shown by discovery of 3,700-million-year-old microbial structures. Nature, 537 (7621), 535-538.

Rapid emergence of life shown by discovery of 3700 million year old microbial structures

Allen P. Nutman[1,5], Vickie C. Bennett[2,5], Clark R. L. Friend[3], Martin J. Van Kranendonk[4,5,6] & Allan R. Chivas[1]

[1]GeoQuEST Research Centre, School of Earth & Environmental Sciences, University of Wollongong, Wollongong, NSW 2522, Australia

[2]Research School of Earth Sciences, Australian National University, Canberra, ACT 0200, Australia,

[3]Glendale, Tiddington, Oxon, OX9 2LQ, UK

[4]School of Biological, Earth and Environmental Sciences, University of New South Wales Australia, Kensington, NSW 2052, Australia

[5] Australian Centre for Astrobiology, University of New South Wales Australia, Kensington, NSW 2052 Australia

[6] Australian Research Council Centre of Excellence for Core to Crust Fluid Systems

Biological activity is a major factor in Earth's chemical cycles, including facilitating CO_2 sequestration and providing climate feedbacks. Thus a key question in Earth's evolution is when did life arise and impact hydrosphere-atmosphere-lithosphere chemical cycles? Until now, evidence for the oldest life on Earth focused on debated stable isotopic signatures of 3,800-3,700 million-year-old (Ma) metamorphosed sedimentary rocks and minerals[1,2] from the Isua supracrustal belt (ISB), southern West Greenland[3]. Here, we show new evidence for ancient life from a newly-exposed outcrop of 3,700 Ma metacarbonate rocks in the ISB that contain 1-4 cm high stromatolites - macroscopically layered structures produced by microbial communities. The ISB stromatolites grew in a shallow marine environment, as indicated by seawater-like rare earth element + yttrium trace element signatures of the metacarbonates, and by interlayered detrital sedimentary rocks with cross-lamination and storm-wave generated breccias. The ISB stromatolites predate by 220 million years the previous most convincing and generally accepted multidisciplinary evidence for oldest life remains in the 3,480 Ma Dresser Formation of the Pilbara Craton, Australia[4,5]. The presence of the ISB stromatolites demonstrates the establishment of shallow marine carbonate production with biotic CO_2 sequestration by 3,700 Ma, near the start of Earth's sedimentary record. A sophistication of life by 3,700 Ma is in accord with genetic molecular clock studies placing life's origin in the Hadean (>4,000 Ma)[6].

Stromatolites are broadly defined as sedimentary structures that are produced by microorganism communities through trapping and binding of sediment, and/or precipitation of carbonate[7]. Stromatolites are the most persistent evidence of life in Earth history, and are known from the present (e.g., Shark Bay, Western Australia) to 3,480 million years ago (Ma) in the rock record[4,5].

Little deformed and weakly metamorphosed 3,480-3,350 Ma sedimentary rocks from the East Pilbara Terrane of the Pilbara Craton (Western Australia) contain the oldest convincing evidence for life on Earth in the form of domical and coniform stromatolites[5,8]. In these cases, a biological origin for stromatolites is supported by morphology[8], stable isotope signatures[9], seawater-like trace element signatures of the dolomitic host rocks[10] and the presence of microfossils[11]. Early life environments in the Pilbara Craton included shallow marine and emergent sedimentary settings, as well as thermal springs. This variety of environments, combined with a diversity of stromatolite forms within individual units, indicates that by 3,480 Ma the biosphere was already diverse, and thus life must have originated significantly earlier[12].

The search for even earlier life is confounded by the scarcity of Eoarchaean (>3,600 Ma) and Hadean (>4,000 Ma) rocks and the strong deformation and high grade metamorphism (500-750°C) that affected them. In most localities this has eliminated primary features within these rocks (‘primary’ here means structures pertaining to the formation of the protolith, prior to superimposed metamorphism)[3]. This is a particular problem in the search for signs of early life in carbonate rocks, due to the propensity of carbonates to undergo ductile deformation and recrystallise as marble during metamorphism and orogeny. Consequently, the search for evidence of life in Eoarchaean rocks has focussed on chemical signatures, such as the isotopic compositions of carbon (as graphite) and iron from metasedimentary rocks, but the origin of these signatures is not unique and their significance as evidence of ancient life remains debated[2,13,14,15]. Most isotopic searches for the oldest evidence of life have targeted the Isua supracrustal belt (ISB) of southern West Greenland, because it contains by far the largest areal extent of diverse Eoarchaean metasedimentary rocks with rare, small areas of low deformation in which primary sedimentary structures are preserved[16].

This contribution presents the discovery of c. 3,700 Ma structures (Fig. 1) interpreted as stromatolites in an ISB outcrop of dolomitic rocks, newly-exposed by melting of a perennial snow patch. The stromatolite discovery locality (Extended Data Fig. 1) is within the hinge of an anticline cored by 3,709 ± 9 Ma andesitic metavolcanic rocks with locally-preserved pillow structures and a maximum metamorphic temperature of c. 550 °C[17,18]. The pillowed metavolcanic rocks are overlain by bedded dolomite-rich metasedimentary rocks and in turn, by interlayered quartzites and metamorphosed banded iron formation that contain rare, small, high Th/U oscillatory-zoned volcano-sedimentary zircons with ages of 3,699 ± 12 and 3,691 ± 6 Ma[3,18]. The term 'dolomite' is used here for compositions ranging from ferroan dolomite to magnesian ankerite.

Most ISB metadolomitic rocks are strongly deformed with quartz + tremolite + calcite ± phlogopite ± muscovite *or* tremolite + dolomite + calcite ± phlogopite ± muscovite mineral assemblages (Extended data Fig. 2a). However, within the c. 30 m by 70 m low strain lacuna discovery locality, there are domains where a CO_2-rich fluid phase was maintained during 550-500°C metamorphism, meaning that quartz and dolomite were still in equilibrium and did not react to form tremolite (Fig. 2a; Extended data Fig. 2b). It is this absence of reaction between dolomite and quartz that aided the preservation of the fine-scale primary structures in these rocks.

At two outcrops in the low strain area are several beds with distinct, 1 to 4 cm high, coniform and apparently low amplitude domical stromatolites interbedded with sedimentary rocks in which several types of depositional structures are displayed, pointing to shallow water conditions are locally preserved. At site 'A' near the edge of the low strain lacuna, coniform to domical stromatolites that occur in three beds (Fig. 1a,b; see Extended Data Figs. 2c, 3 and for a more detailed description). The outcrop preserves these structures only in cross section, and their profiles are triangular to dome-shaped, the former geometry having a sharp apex at the top and a flat base that is consistent with bedding top directions in associated metasedimentary rocks (see below). The three- dimensional geometry of the stromatolites is as elongated, commonly asymmetrical cones or domes, as demonstrated by images of a sawn block from the outcrop (Extended Data Fig. 4. Some of the coniform structures are asymmetrical, with one of their sides steeper than the other, similar to the asymmetry displayed by some better preserved stromatolites from the c. 3,400 Ma Strelley Pool Formation and c. 2,030 Ma Wooly Dolomite (Figs. 1c, 1d: e.g., Van Kranendonk[12]).

Amphibolite facies metamorphism has caused recrystallisation of the stromatolites to 100-200 μm granoblastic aggregates of dolomite + quartz (Extended Data Fig. 4a) that mostly obscures original fine-scale growth structures. Nonetheless, on outcrop the outer margins of site 'A' stromatolites show internal lamination that is continuous across the crests of the structures (Figs. 1a,b). Additionally, backscattered electron imaging near the crest of a structure demonstrates preservation of a millimetre-scale compositional layering parallel to the upper bounding surface of the stromatolite, despite Ostwald ripening during recrystallisation giving the current granoblastic texture (Extended Data Figure 3). Both the outcrop exposures (Figs 1a, 1b) and cut surfaces of the sawn sample (Extended Data Fig. 4) show that thin, horizontal sedimentary beds onlap the dipping sides of the stromatolites in a similar fashion as documented for 3,400 Ma Strelley Pool Formation stromatolites and indeed stromatolites of any age[12]. Significantly, Ti and K abundances, which are indicative of phlogopite content reflecting an original muddy component of the sediment, are lower by an order of magnitude in the stromatolites relative to the adjacent sediment (Extended Data Fig. 4c). This supports the stromatolites having grown by microbial activity rather than by abiogenic precipitation of mineral crusts.

At site 'B', lower amplitude (1 cm), more closely-spaced, domical stromatolites are outlined at the top of a metadolomite unit where it is overlain by bedded, cross-laminated metasandstones (quartz + minor dolomite + phlogopite ± muscovite; Figs. 2b,c, Extended Data Fig. 2d and Table 1). Bedding in the sedimentary rock immediately above the metadolomite is defined by draping phlogopite + dolomite laminae and contrasts sharply with the well-developed, centimetre-scale cross-stratification present in the overlying quartz-rich metasandstones that gives a way-up indicator. The cross-lamination is hummocky, with clearly-developed erosional surfaces. This type of depositional structure is most widely developed where there is repeated change of current direction, such as controlled by tides. This bedding style is distinct from, and unaffected by, the underlying domical structures and represents one of the best-preserved sedimentary structures in the Isua supracrustal belt (Figs. 2b, c; Extended Data Fig. 2b).

Low deformation lacuna site 'C' preserves a 30 cm thick breccia lens in dolomite-rich metasedimentary rocks is associated with dolostone (Fig. 2d). The breccia consists of randomly orientated, angular clasts of bedded quartz-rich and carbonate-rich metasedimentary rocks in a finer grained dolomite + quartz matrix. Some clasts contain abundant hyalophane (Extended Data Table 1), a barium-rich feldspar that commonly develops in metamorphosed dolomitic, marly, evaporitic rocks[19]. The random orientation of the clasts, combined with that some showing plastic deformation, resembles tempestite breccias formed in shallow marine environments where partially lithified material is ripped up and redeposited by deepening of the wave base during storms. This shallow water setting contrasts with evidence that sedimentary rocks in other tectonic packages of the ISB formed in deeper water conditions[2,16]. This reinforces the diverse origins of different packages of rocks in the belt[18].

The barium-rich character of some layers of the dolomitic succession (up to 1 wt% BaO) now represented by halogen-rich barian phlogopite ± barian muscovite ± hyalophane (Extended Data Table 1), support periodic evaporitic conditions and the generally shallow water environment. Tempestite breccias formed by wave action require ice-free waters. This, together with the absence of glaciogenic diamictites in the ISB, indicates an equable climate at 3,700 Ma that, under the faint young Sun, was probably supported by a more CO_2- and/or CH_4-rich atmosphere[20,21].

Locality 'A' stromatolites and the bedded metadolomite interlayered with them display seawater-like rare-earth-element plus yttrium (REE+Y) signatures with diagnostic positive Y and La anomalies and low total REE contents (Fig. 3, Extended Data Table 2 and Fig. 4). This REE+Y signature is preserved in even the most Ti-Al rich 'marly' layer (analysis A-2 Fig. 3, Extended Data Table 2) and indicates a marine, rather than a hydrothermal, lacustrine or estuarine environment[10]. The lack of a discernible negative Ce anomaly (Fig. 3) is consistent with reducing conditions of deposition. The presence of accessory phlogopite ± muscovite in the bedded dolomites indicates a minor potassic input, typical of that derived from alteration, as indicated additionally by the K-enrichment in altered ISB basalts[22]. Significantly, stromatolitic structures are compositionally distinct from the interlayered bedded sedimentary rocks at the studied localities, as revealed by petrographic observations and geochemical traverses (Extended Data Table 2, Figs. 2b, 3, 4c).

Stromatolitic metacarbonates have uniform carbon and oxygen isotopic values of $\delta^{13}C_{VPDB}$ = +1.4 ± 0.1 and $\delta^{18}O_{VSMOW}$ = +18.4 ± 0.1 (1σ; Extended Data Table 3). The closed system metamorphism of these rocks, and absence of aqueous fluids leading to decarbonation reactions, suggests that primary dolomite carbon isotopic ratios would not have been significantly isotopically modified during metamorphism. The carbon isotopic compositions are consistent with precipitation from a carbonate pool from which carbon with a low $^{13}C/^{12}C$ ratio had been extracted, assuming a modern atmosphere starting isotopic composition. In modern stromatolites, this is the result of early carbonate cement precipitation in the presence of microbial communities that fixed carbon dioxide to organic matter. The Isua stromatoliteconstructing communities thus show possible evidence of an autotrophic carbon-fixing metabolism. The $\delta^{18}O_{(VSMOW)}$ values are similar to those for stromatolitic dolomite in 3,480-3,400 Ma Pilbara stromatolites formed in marginal marine to evaporitic conditions[23]. Given the contrast in metamorphic grade of the Pilbara and Isua samples (sub-greenschist versus low-amphibolite facies), this suggests that the Isua sample oxygen isotopic signatures reflect processes during deposition or during diagenetic cement formation shortly afterwards.

Several lines of evidence *combine* to indicate the biogenicity of the proposed Isua stromatolites:

(i) Sharp, steep-sided walls on Isua stromatolites are onlapped by adjacent marine dolomitic sediment, indicative of growth of the stromatolites above the sediment-water interface (cf. Van Kranendonk[12]). The diversity of Isua forms matches some Palaeoarchaean stromatolites (Fig. 1).

(ii) The presence of originally low temperature dolomite, which requires microbial activity for precipitation[24,25].

(iii) The stromatolite trace element compositions, including positive La anomalies, Y/Ho ratios approaching that of modern seawater, light rare earth element depletions relative to average shale, and small positive Eu anomalies consistent with other Archaean orthochemical sedimentary rocks. This precludes formation of these structures as abiotic hydrothermal exhalites.

(iv) Internal lamination. A key feature demonstrating the biogenic origin of ancient stromatolites is a laminated growth pattern that is independent from structures formed purely by physical sedimentary processes[7]. Although recrystallised, the stromatolites preserve relicts of convex-upwards lamination (Fig. 1 and Extended Data Fig. 4) across their culminations, indicating they were not formed as dewatering structures.

Nonetheless, suggestions that some peaked or domical stromatolite-like structures could be abiogenic mineral accumulations[26] should be considered for the structures described here. Importantly, four significant morphological differences exist between biological stromatolites and abiological crusts, as also pointed out for c. 3400 Ma coniform stromatolites from the Pilbara Craton[8]. (i) Depending on the material used in abiological experiments or analogues, only either dome-shaped or peak-shaped structures form, but never the two together as observed from the Isua, and many younger, stromatolites[12]. (ii) Regardless of material used, abiogenic laminae thicken in troughs, whereas in the Isua stromatolites, laminae are of minimal thickness, or are not developed in troughs. (iii) Abiogenic peaked structures do not form inclined, asymmetrical structures, whereas some Isua coniform stromatolites do. (iv) Abiogenic peaked structures form irregular projections that grow normal to the growth surface, whereas such projections are absent from Isua stromatolites. On these grounds, we rule out an abiologic origin for Isua stromatolites.

The recognition of c. 3,700 Ma biogenic stromatolites within Isua dolomites indicates that near the start of the preserved sedimentary record, atmospheric CO_2 was being sequestered by biological activity[27]. The complexity and setting of the Isua stromatolites points to sophistication in life systems at 3,700 Ma, similar to that displayed by 3,480-3,400 Ma Pilbara stromatolites[4,8,12]. This implies that by c. 3,700 Ma life already had a considerable prehistory, and supports model organism chronology that life arose during the Hadean (>4,000 million years ago)[6]. A shallow-water depositional environment is not necessary to conclude biogenicity, since deep-water microbialites and stromatolites are known. However, a shallow water environment is supported by the associated sedimentary structures such as cross-lamination and tempestite breccias.

Online Content Methods, along with any additional Extended Data display items and Source Data, are available in the online version of the paper; references unique to these sections appear only in the online paper.

Acknowledgements Support provided by Australian Research Council grant DP120100273 and the GeoQuEST Research Centre, University of Wollongong (UOW). David Wheeler, UOW, is thanked for technical assistance in carbon and oxygen isotopic analysis. Leslie Kinsley, Research School of Earth Sciences, Australian National University is thanked for assistance with LA-ICP-MS data acquisition. David Adams of the Department of Earth & Planetary Sciences, Macquarie University is thanked for assistance with mineral analyses. Mitchell Nancarrow of the Electron Microscopy Centre, UOW is thanked for assistance with SEM-imaging and mineral analyses. Patricia Gadd of the Australian Nuclear Science and Technology Organisation is thanked for undertaking ITRAX analyses. MJVK acknowledges support by the University of New South Wales. This is Publication Number XXYY of the Australian Research Council Centre of Excellence for Core to Crust Fluid Systems.

Author Contributions A.P.N and V.C.B. undertook field work, acquisition of geochemical data and interpretation of the results. C.R.L.F. undertook fieldwork and interpretation of the results. M.J.V.K. interpreted the Isua stromatolite morphology and compared them with those from the Pilbara region of Western Australia and supplied the photographs for Figures 1c, 1d. A.R.C. acquired and interpreted the stable isotope data. A.P.N. wrote the paper and all authors read and contributed comments to the work.

Author information Reprints and permissions information is available at www.nature.com/reprints. The authors declare no competing financial interests. Readers are welcome to comment on the online version of the paper. Correspondence and requests for materials should be addressed to A.P.N. (anutman@uow.edu.au).

References

1 Schidlowski, M. Appel, P.W.U., Eichmann, R. & Junge, C.E. Carbon isotope geochemistry of the 3.7 x 10^9 –yr old Isua sediments, West Greenland: implications for the Archaean carbon and oxygen cycles. *Geochimica et Cosmochimica Acta* **43**, 189-199 (1979).

2 Rosing, M.T. ^{13}C-depleted carbon microparticles in >3700 Ma sea-floor sedimentary rocks from West Greenland. *Science* **283**, 674-676 (1999).

3 Nutman, A.P. & Friend, C.R.L. New 1:20000 geological maps, synthesis and history of the Isua supracrustal belt and adjacent gneisses, Nuuk region, southern West Greenland: A glimpse of Eoarchaean crust formation and orogeny. *Precambrian Research*, **172**, 189-211 (2009).

4 Walter, M.R., Buick, R. & Dunlop, S.R. Stromatolites 3,400-3,500 Myr old from the North Pole area, Western Australia. *Nature* **284**, 443-445 (1980).

5 Van Kranendonk, M.J., Philippot, P., Lepot, K., Bodorkos, S. & Pirajno, F. Geological setting of Earth's oldest fossils in the c. 3.5 Ga Dresser Formation, Pilbara craton, Western Australia. *Precambrian Research* **167**, 93-124 (2008).

6 Hedges, S.B. The origin and evolution of model organisms. *Nature Review Genetics* **3**, 838-849 (2002).

7 Riding, R. The nature of stromatolites: 3,500 million years of history and a century of research. In J.Reitner et al. (editors) Advances in Stromatolite Geobiology, Springer-Verlag, Berlin, 29-74 (2011).

8 Allwood, A.C., Walter, M.R., Kamber, B.S., Marshall, C.P., Burch, I.W. Stromatolite reef from the Early Archaean era of Australia. *Nature* **441,** 714-718 (2006).

9 Philippot, P. Van Zuilen, M. Lepot, K., Thomazo, C., Farquhar, J. & Van Kranendonk, M.J. Early Archean microorganisms preferred elemental sulfur, not sulfate. *Science* **317**, 1534-1537 (2007).

10 Van Kranendonk, M.J., Webb, G.E. & Kamber, B.S. Geological and trace element evidence for marine sedimentary environment of deposition and biogenicity of 3.45 Ga stromatolite carbonates in the Pilbara Craton, and support for a reducing Archean ocean. *Geobiology* **1,** 91-108 (2003).

11 Sugitani, K., Lepot, K., Mimura, K., Van Kranendonk, M.J., Oehler, D. & Walter, M.R. Biogenicity of morphologically diverse carbonaceous microstructures from the ca. 3400 Ma Strelley Pool Formation, in the Pilbara Craton, Western Australia. *Astrobiology* **10**, 899–920 (2010).

12 Van Kranendonk, M.J. Stromatolite morphology as an indicator of biogenicity for Earth's oldest fossils from the 3.5-3.4 Ga Pilbara craton, Western Australia, in Reitner, J., Queric, N.-V. and Arp, G., eds., Advances in Stromatolite Geobiology: Lecture Notes in Earth Sciences, 131, Berlin, Springer, p. 517-534 (2011).

13 Mojzsis, S.J., Arrhenius, G., McKeegan, K.D., Harrison, T.M., Nutman, A.P. & Friend, C.R.L. Evidence for life on Earth before 3800 million years ago. *Nature* **270**, 43-45 (1996).

14 Van Zuilen, M., Lepland, A. & Arrhenius, G. Reassessing the evidence for the earliest traces of life. *Nature* **418**, 627-630 (2002).

15 Dauphas, N., van Zuilen, M., Wadhwa, M., Davis, A.M., Marty, B. & Janney, P.E. Clues from Fe isotope variations on the origin of early Archean BIFs from Greenland. *Science* **306**, 2077-2080 (2004).

16 Nutman, A.P., Allaart, J.H., Bridgwater, D. Dimroth, E. & Rosing, M.T. Stratigraphic and geochemical evidence for the depositional environment of the early Archaean Isua supracrustal belt, southern West Greenland. *Precambrian Research* **25**, 365-396 (1984).

17 Rollinson, H. Metamorphic history suggested by garnet-growth chronologies in the Isua Greenstone Belt, West Greenland. *Precambrian Research* **126**, 181–196 (2003).

18 Nutman, A.P., Bennett, V.C. & Friend, C.R.L. The emergence of the Eoarchaean proto-arc: evolution of a c. 3700 Ma convergent plate boundary at Isua, southern West Greenland. In: Roberts, N. M. W., Van Kranendonk, M., Parman, S., Shirey, S.& Clift, P. D. (eds) Continent Formation Through Time. The Geological Society, London, Special Publications **389**, 113-133 (2015).

19 Feneyrol, J., Ohnenstetter, D., Giuliana, G., Fallick, A.E., Rollion-Bard, C., Robert, J.L. & Malisa, E.P. Evidence of evaporites in the genesis of the vanadian grossular 'tsavorite' deposit in Namalulul, Tanzania. *The Canadian Mineralogist* **50**, 745-769 (2012).

20 Nutman, A.P., Bennett, V.C. & Friend, C.R.L. Waves and weathering at 3.7 Ga. Geological evidence for an equable terrestrial climate under the faint early Sun. *Australian Journal of Earth Sciences* **59**, 167-176 (2012).

21 Walker, J.C.G., Hays, P.B. & Kasting, J.F. A negative feedback mechanism for the long-term stabilization of the earth's surface temperature. *Journal of Geophysical Research* **86**, 9776–9782 (1981).

22 Polat, A., Hofmann, A.W., Münker, C., Regelous, M. & Appel, P.W.U. Contrasting geochemical patterns in the 3.7-3.8 Ga pillow basalts cores and rims, Isua greenstone belt, Southwest Greenland: Implications for post-magmatic alteration. *Geochimica et Cosmochimica Acta* **67,** 441-457 (2003).

23 Lindsay, J.F., Brasier, M.D., McLoughlin, N., Green, O.R., Fogel, M., Steele, A. & Mertzman, S.A., The problem of deep carbon – an Archean paradox. *Precambrian Research* **143**, 1-22 (2005).

24 Vasconcelos, C., McKenzie, J.A., Bernasconi, S., Grujic, D. & Tien, A.J. Microbial mediation as a possible mechanism for natural dolomite at low temperatures. *Nature* **377,** 220-222 (1995).

25 Roberts, J.A., Bennett, P.C., González, L.A., Macpherson, G.L. & Milliken, K.L. Microbial precipitation of dolomite in methanogenic groundwater. *Geology* **32**, 277-280 (2004).

26 Grotzinger, J.P. & Rothman, D.H.. An abiotic model for stromatolite morphogenesis. *Nature* **383**, 423-425 (1996).

27 Nutman, A.P., Friend, C.R.L., Bennett, V.C., Wright, D. & Norman, M.D. ≥3700 Ma pre-metamorphic dolomite formed by microbial mediation in the Isua supracrustal belt (W. Greenland): Simple evidence for early life? *Precambrian Research* **183**, 725-737 (2010).

28 Müller, S.G., Krapez, B., Barley, M.E., & Fletcher, I.R.. Giant ore deposits of the Hamersley province related to the breakup of Paleoproterozoic Australia: New insights from in situ SHRIMP dating of baddelyite in mafic intrusions. *Geology* **33,** 577-580 (2005).

29 McClennan, S.M. Rare earth elements in sedimentary rocks: influence of provenance and sedimentary processes. In: Geochemistry and Mineralogy of Rare Earth Elements

(eds. Lipin, B.R., and McKay, G.A.), Mineralogical Society of America, Washington, DC, USA, p. 169-200 (1989)

30 Friend, C.R.L., Nutman, A.P., Bennett, V.C. & Norman, M.D. Seawater-like trace element signatures (REE+Y) of Eoarchaean chemical sedimentary rocks from southern West Greenland, and their corruption during high grade metamorphism. *Contributions to Mineralogy and Petrology* **155**, 229-246 (2008).

Figure legends

Figure 1. **a,** Site 'A' stromatolites. Image is inverted because layering is overturned in a fold. **b,** Interpretation of frame a, with isolated stromatolite (strom) and aggregate of stromatolites (stroms). Locally, lamination is preserved in the stromatolites (blue lines). Layering in the overlying sediment (red lines) onlaps onto the stromatolite sides. A weak tectonic foliation is indicated (green lines). **c,** Asymmetrical stromatolite and **d,** low amplitude, linked domical stromatolites from the 2031 ± 6 Ma Wooly Dolomite of the Wyloo Group, Western Australia[28]. The lens cap in both is 4 cm in diameter. Image **c** is left-right-reversed for comparison with panels **a,b**.

Figure 2. **a,** SEM image showing quartz (qtz) and dolomite (dol) equilibrium, with phlogopite (phlog) and pyrite altered to magnetite (py-mag). **b,** Site 'B' structures. Dolostone (dolostone) has domical interface with cross-laminated dolomitic sandstone (dol + qtz; image top). The red arrow indicates erosional scouring of a layer. Bar 'C' is site for thin section in **c**. Pen for scale, bottom of image. **c,** Photomicrograph from the domical interface, showing draping of phlogopite + dolomite layers (blue arrows) within sediment immediately above the dolostone domical structures . **d,** Site 'C' breccia with jumbled clasts, showing layered chert (ch) and dolomite (dol) clasts.

Figure 3. PAAS-normalised (post-Archaean average shale)[29] rare earth element and yttrium plot. Site 'A' sample G12/96 Isua stromatolite dolomites and bounding sedimentary rocks are *in situ* Laser-Ablation ICP-MS analyses from the block shown in Extended Data Fig. 5. A c. 3,700 Ma Isua banded iron formation sample[30] and an East Pilbara dolomitic stromatolite[10] are shown for comparison. Diagnostic of the seawater-like signature are positive yttrium (Y) and lanthanum (La) anomalies. See Methods for analytical methods and Extended Data Table 2 for analyses.

Methods

Electron probe analysis

Microprobe mineral analyses were carried out on polished thin sections utilizing a fully automated, Cameca SX100 electron microprobe at Macquarie University, fitted with five wavelength dispersive spectrometers (WDS). The operating conditions were: accelerating voltage 15 kV; beam current 20 nA and the beam size was focussed to 20 µm for carbonates and 5 µm for other minerals.

Major and trace element analysis

For samples G11/63 and -72 rare trace element concentrations were analysed commercially at the Australian Laboratory Services (ALS) at Brisbane, Australia, by inductively coupled plasma–mass spectroscopy (ICP-MS) on fused glass discs. Site 'A' sample G12/96 Isua stromatolite dolomite *in situ* trace element analyses were acquired by ICP-MS at the Australian National University using a Lambda Physik 193 nm UV excimer laser-ablation system, equipped with a dual-volume ANU HelEx chamber, coupled to a Varian 820 quadrupole ICP-MS. After laser pre-cleaning, data were acquired for 39 masses by ablation along a continuous transect across the sample perpendicular to bedding using an 800 µm by 20 µm slit moving at 10 µm per second. Laser operating conditions were 5 HZ, 24.9 MJ and 17.0 KV. Data representing the lithologic variations above, across and below the stromatolite were obtained by combining analyses into eleven segments (Extended data Fig. 4). NIST 612 glass was used for calibration and an in-house dolomite standard was analysed as a quality control standard.

Carbon and oxygen isotopes

The ankeritic dolomite samples were reacted with 105% H_3PO_4 at 90°C in an acid-on-individual carbonate MultiPrep system attached to a PRISM III mass spectrometer in the geochemical laboratories at the University of Wollongong. The raw $\delta^{18}O$ values in the Table refer to the composition of the evolved CO_2 compared to that extracted from calcite from NBS-18 ($\delta^{18}O_{VSMOW}$ = +7.19) and NBS-19 ($\delta^{18}O_{VSMOW}$ = +28.64). The corrected values ($\delta^{18}O_{VSMOW}$corr) allow for the difference (using the VSMOW scale) between 90°C acid-liberated CO_2 from calcite and ankeritic dolomite (measured composition $Ca_{50}Mg_{30}(Fe,Mn)_{20}$; i.e. 60% dolomite, 40% ankerite end members), for which an offset of 0.92‰ was applied[1]. The calculated $\delta^{18}O$ value of water in equilibrium with the dolomitic samples was derived using a temperature of 525°C and a fractionation factor at this temperature for dolomite-water of 3.6‰ – extrapolation from Northrop and Clayton[2], as in Friedman and O'Neil[3]. Thus $\delta^{18}O_{VSMOW}$ H_2O = 18.4-3.6 = +14.8‰. This value is within the range common for metamorphic water ($\delta^{18}O_{VSMOW}$ = +3 to +20‰)[4].

References

1 Rosenbaum, J. & Sheppard, S.M.F. An isotopic study of siderites, dolomites and ankerites at high temperatures. *Geochimica et Cosmochimica Acta* **50**, 1147-1150 (1986).

2 Northrop, D.A. & Clayton, R.N. Oxygen-isotope fractionations in systems containing dolomite. *Journal of Geology* **74**, 174-196 (1966).

3 Friedman, I. & O'Neil, J.R. Compilation of stable isotope fractionation factors of geochemical interest, Chapter KK. Data of Geochemistry. U.S. Geological Survey Professional Paper 440-KK (1977).

4 Sheppard, S.M.F. Characterization and isotopic variations in natural waters. *Reviews in Mineralogy* **16**, 165-183 (1986).

Extended Data Figure Captions and text-only for first page

(Text for first page of Extended Data)

Petrographic Descriptions

Locality 'A' stromatolite fabrics and layering: This locality is near the edge of the low strain lacuna and hence there is a weak foliation. This is at a high angle to the primary compositional layering (Figs. 1a,b; Extended Data Fig. 4). Related to this there is also minor incursion of hydrous fluid along grain boundaries, leading to patchy development of alteration selvedges on some dolomite grains. Extended Data Figure 4a,b shows a montage of all four sides of a block sawn from the outcrop. The stromatolite structures have flat bases with conical tops in cross section. Although the stromatolite core areas are largely recrystallised and structureless with only vestiges of layering, the outer margins show internal lamination that is continuous across the crests of the structures (Figs. 1a,b). Subtle depositional layering and diagenetic structures in younger non-metamorphosed carbonate sedimentary rocks can be revealed by cathodoluminescence imaging. However, in the case of the Isua stromatolites, 550-500°C metamorphic recrystallisation has given a rise to a granoblastic mosaic of 100-200 µm dolomite + quartz that would have destroyed any depositional cathodoluminescence contrasts between layers. Despite this, SEM backscatter electron imaging reveals a subtle layering preserved on a millimetre scale (grey scale image analysis, with quartz and dolomite appearing with different brightness; Extended Data Fig. 3). This layering revealed by SEM imagery is the same magnitude as subtle layering preserved in younger non-metamorphosed stromatolites (e.g. Figs. 1c,d). This internal lamination is important, as it precludes the structures having formed by dewatering, as this produces a central axial zone that cuts across and disrupts lamination. The sawn block (Extended Data Fig. 4a,b) shows that thin sedimentary beds that onlap the sides of the stromatolites in a similar fashion as documented for 3,400 Ma Strelley Pool Formation stromatolites[12].

Locality 'B' stromatolite fabrics and layering: At least one, and in some places two, thick laminations are preserved draping the observed stromatolites, and these laminations may represent internal fabrics that were present throughout the structures prior to pervasive recrystallisation. These laminations thicken and thin along their length, indicating that they were not isopachous crusts. Some of these laminations are inclined relative to underlying bedding by up to 40 degrees, significantly greater than the angle of repose for loose sediment. This suggests that these laminations were at least partially stabilized by cohesive microbial mats. Local peaks and crenulations are also present in the uppermost lamination with no apparent corresponding underlying relief, consistent with a biological origin but not a purely physical sedimentary origin.

(Caption on page 2 of Extended Data)

Extended Data Figure 1. **a**, Geological map covering the described localities. The outcrops for localities 'A', 'B' and 'C' are indicated. **b**, position of locality in the Isua supracrustal belt. **c**, Panoramic view towards the southeast over the described localities. In the foreground are the banded iron formation and chert outcrops in the northwest corner of the map **a**. The 15-20 m thick Ameralik dyke forms the skyline.

(Caption on page 3 of Extended Data)

Extended Data Figure 2. **a,** Thin section of calc-silicate rocks ~5m south of site 'A'. The strain is still low, but there was ingress of an H_2O-rich fluid phase during metamorphism. Tremolite (green) is developed extensively in the left hand side of the section, from reaction between dolomite and quartz in the presence of the H_2O-rich fluid. The original sedimentary layering (vertical within the slide) is severely disrupted by the tremolite growth, with development of a foliation orientated from lower left to upper right. **b,** Thin section from site 'B' where quartz and dolomite are still in equilibrium, because a CO_2-rich fluid phase was maintained during metamorphism. Fine scale sedimentary structures are preserved (approximately horizontal across the slide). Foliation is absent. Both thin sections are shown at the same scale and are approximately 2 cm wide. **c,** Overview of site 'A'. Image inverted because outcrop is in an overturned fold limb. The red rectangle is the area shown in Figures 1a,b. The two red parallel lines indicate the sawn block in Extended Data Fig. 5. The red arrows point to three layers with stromatolites. Field of view is 2 metres. **d,** Overview of site 'B'. The detailed area shown in the article Figures 2b,c is indicated by a red arrow.

(Caption on page 4 of Extended Data)

Extended Data Figure 3. Stromatolite structure from site 'A'. (**a**) SEM backscattered electron image of an area near the top of the stromatolite shown in frame (c). Variation in brightness is governed by quartz (duller) versus dolomite (brighter) grains. A subtle millimetre-scale layering is visible running horizontally across the image, i.e. parallel to the top of the stromatolite. This was investigated further by examining the relative greyscales of the pixels forming the right hand side of the image (red box in frame **a**). The other side of this image was not used in pixel analysis, because of the black field (beyond the edge of the scanned sample). (**b**) Shows the variation in grey scale. **c**, Indicates the sampling sites for carbonate oxygen and carbon isotope analysis (Extended Data Table 3).

(Caption on page 5 of Extended Data)

Extended Data Figure 4. Locality ‘A’ sawn block. **a**, Montage of four sides of block. **b**, Sampling site pre- and post-removal of block. **c**, Location of analyses A-1 to A-11 (Extended Data Table 2). Note the onlap of this horizontal bedding to the stromatolite margin on the first block side. **d,** X-Ray Fluorescence ITRAX scans of a locality ‘A’ stromatolite culmination and the laterally-equivalent horizon. Scans are given as relative counts per second on the relevant X-Ray peak. This shows the featured stromatolite layer (‘d’ on the image of the rock slice) has much lower Ti and K abundances (denoting the phlogopite proxy for a lower mud content) compared with the layers above and below.

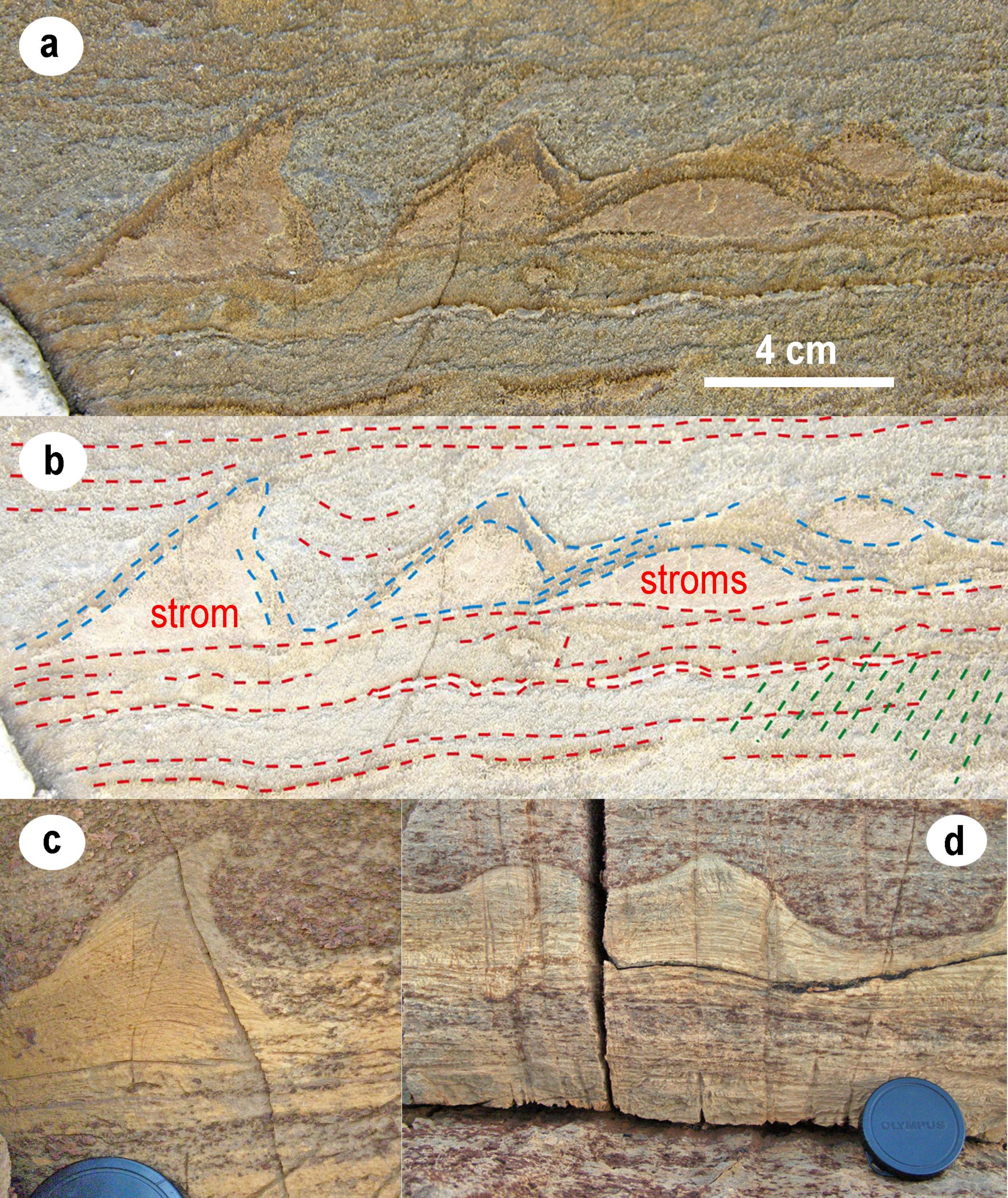
a
4 cm
b
strom
stroms
c
d
OLYMPUS

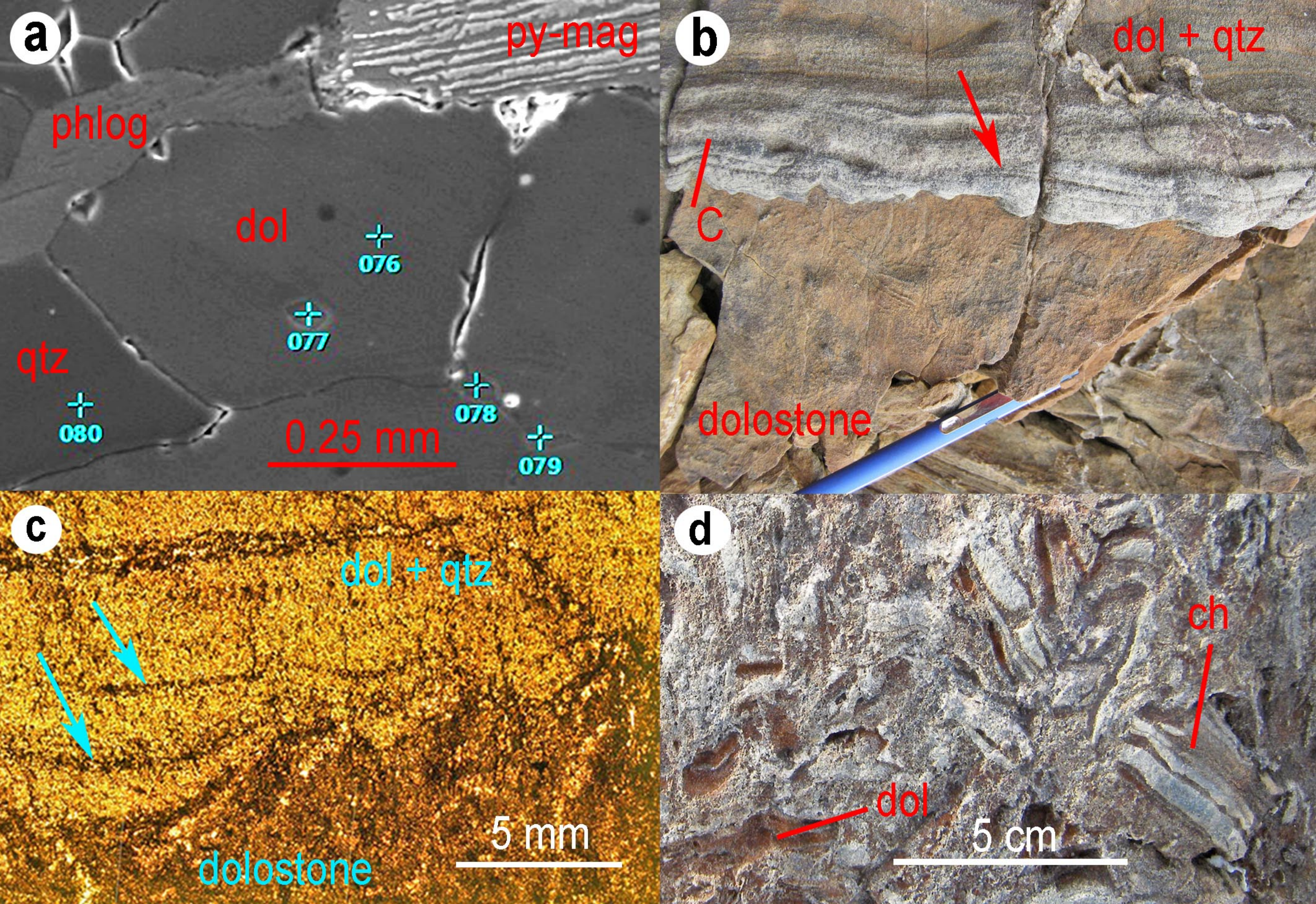

a
py-mag
phlog
dol
076
077
qtz
080
078
079
0.25 mm
b
dol + qtz
C
dolostone
c
dol + qtz
dolostone
5 mm
d
ch
dol
5 cm

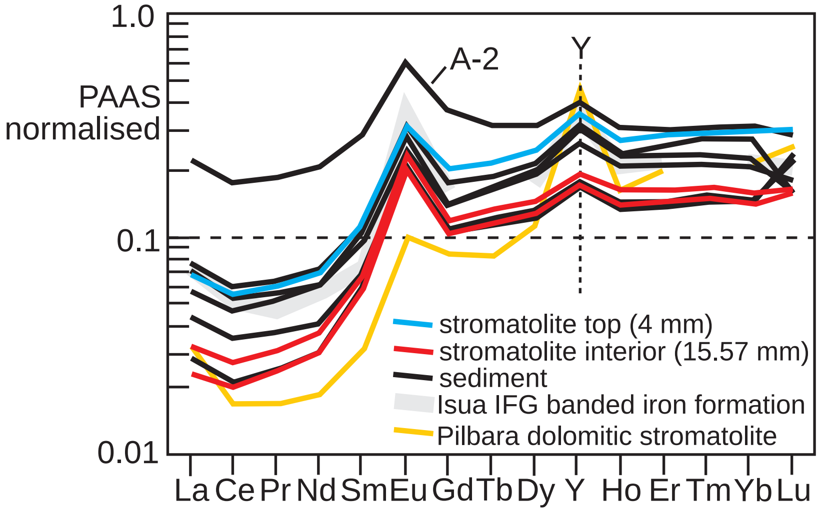

1.0
PAAS
normalised
0.1
0.01
A-2
Y
stromatolite top (4 mm)
stromatolite interior (15.57 mm)
sediment
Isua IFG banded iron formation
Pilbara dolomitic stromatolite
La Ce Pr Nd Sm Eu Gd Tb Dy Y Ho Er Tm Yb Lu

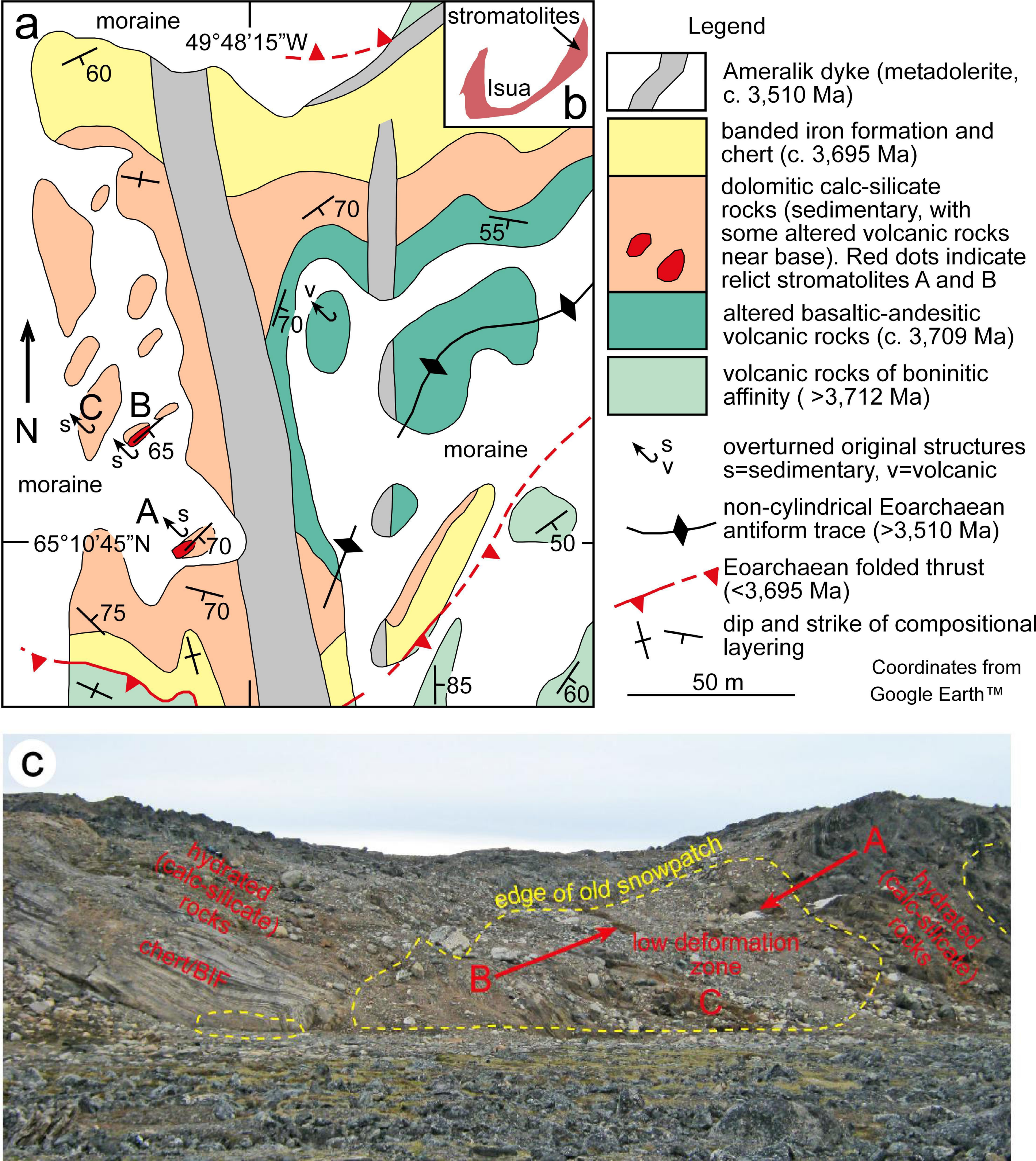
a
moraine
49°48'15"W
60
70
55
v
70
C
B
s
s
65
N
moraine
A
s
65°10'45"N
70
75
70
moraine
50
85
60
b
stromatolites
Isua
Legend
Ameralik dyke (metadolerite, c. 3,510 Ma)
banded iron formation and chert (c. 3,695 Ma)
dolomitic calc-silicate rocks (sedimentary, with some altered volcanic rocks near base). Red dots indicate relict stromatolites A and B
altered basaltic-andesitic volcanic rocks (c. 3,709 Ma)
volcanic rocks of boninitic affinity (>3,712 Ma)
s
v
overturned original structures s=sedimentary, v=volcanic
non-cylindrical Eoarchaean antiform trace (>3,510 Ma)
Eoarchaean folded thrust (<3,695 Ma)
dip and strike of compositional layering
50 m
Coordinates from Google Earth™
c
hydrated (calc-silicate) rocks
chert/BIF
edge of old snowpatch
A
B
low deformation zone
C
hydrated (calc-silicate) rocks

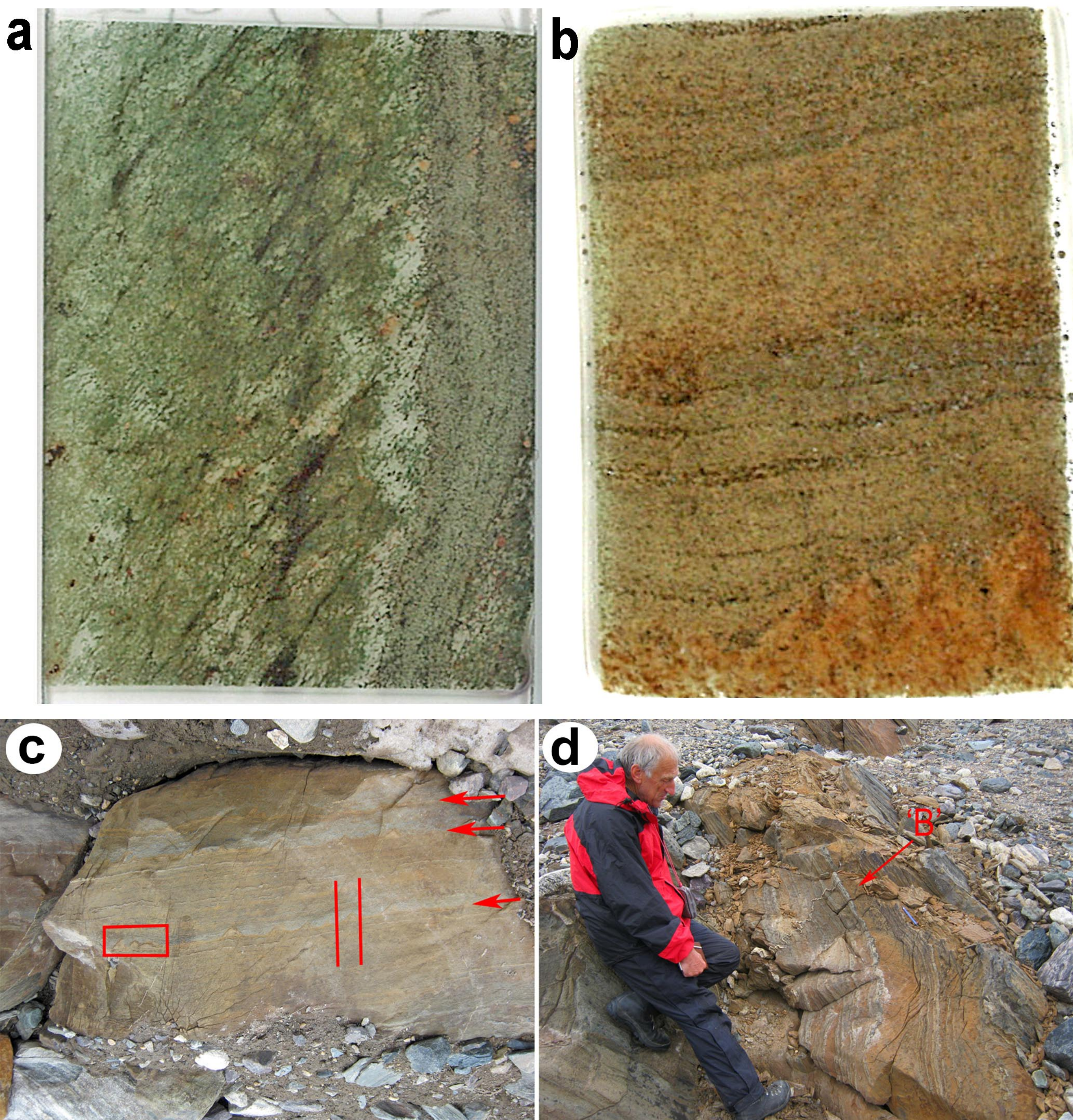
a
b
c
d
'B'

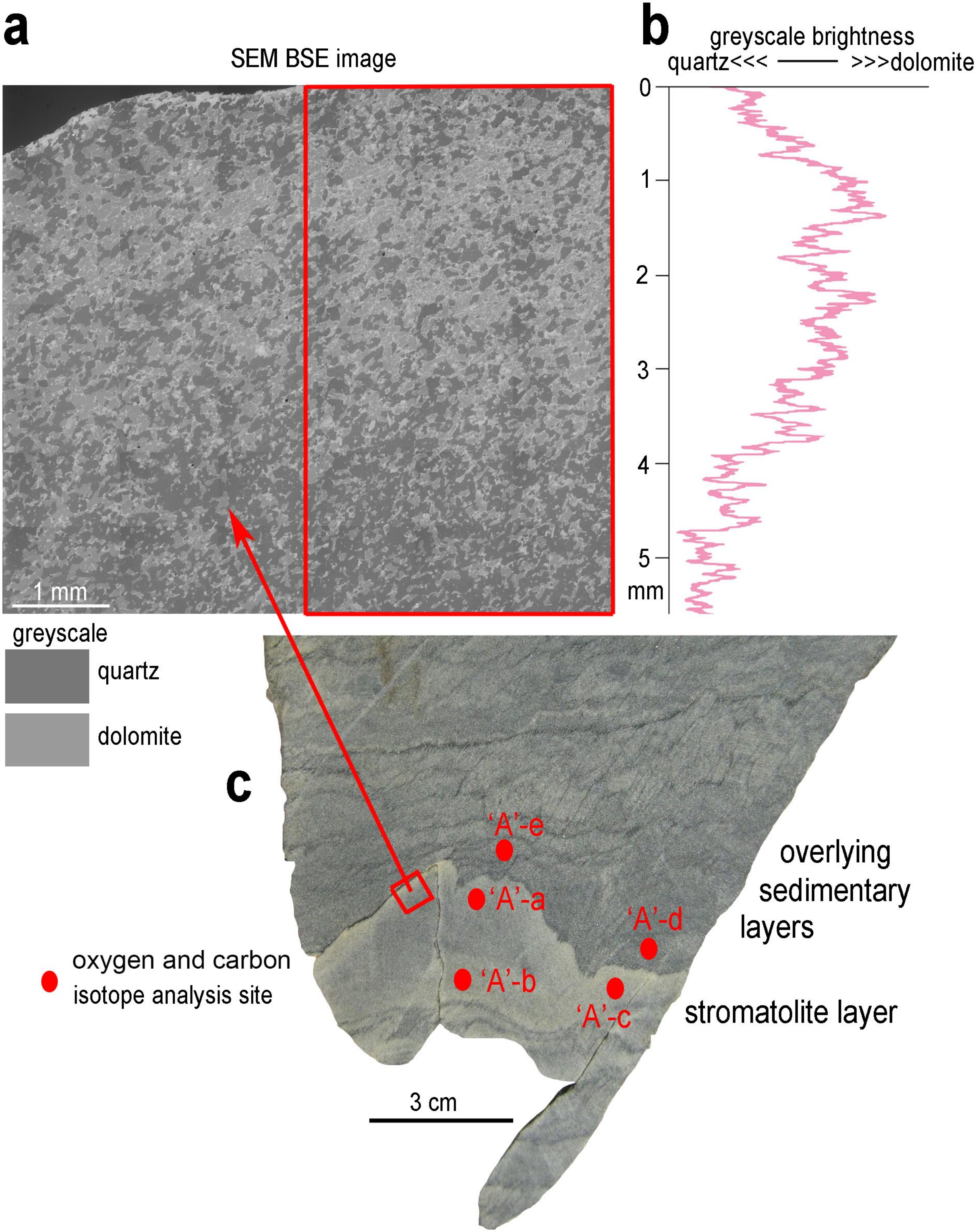

a
SEM BSE image
1 mm
b
greyscale brightness
quartz<<< >>>dolomite
0
1
2
3
4
5
mm
greyscale
quartz
dolomite
c
'A'-e
'A'-a
'A'-d
'A'-b
'A'-c
overlying sedimentary layers
stromatolite layer
oxygen and carbon isotope analysis site
3 cm

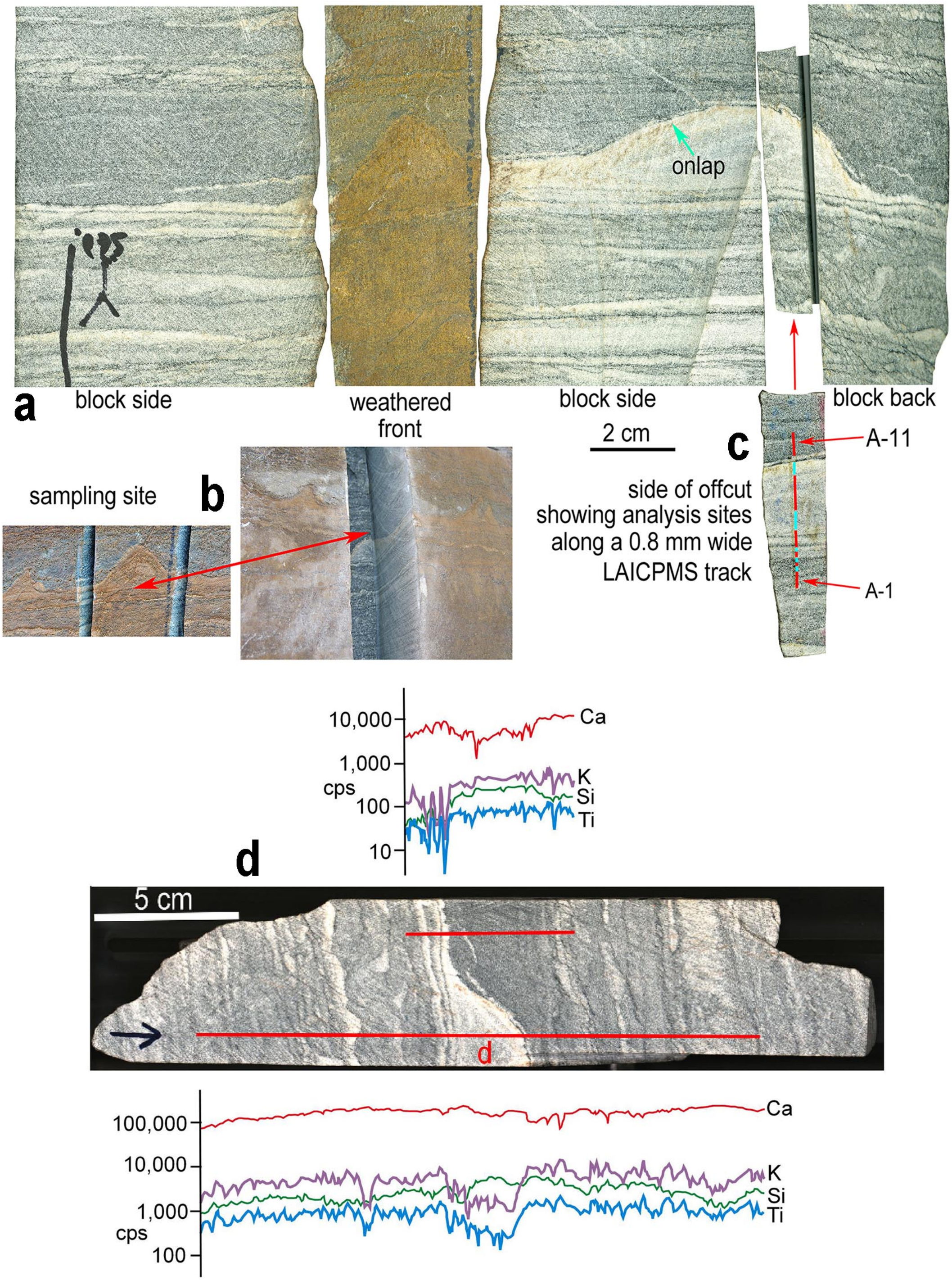
onlap
a
block side
weathered
front
block side
block back
2 cm
c
A-11
A-1
side of offcut
showing analysis sites
along a 0.8 mm wide
LAICPMS track
sampling site
b
10,000
1,000
cps
100
10
Ca
K
Si
Ti
d
5 cm
d
100,000
10,000
1,000
cps
100
Ca
K
Si
Ti

	B musc-1	B phlg-1	B phlg-2	B phlg-3	B phlg-4	B phlg-5	B phlg-6	B phlg-7	B dol-1	B dol-2	B dol-3	B dol-4	B dol-5
	MU-WDS	MU-WDS	MU-WDS	MU-WDS	MU-WDS	MU-WDS	MU-WDS	MU-WDS	MU-WDS	MU-WDS	MU-WDS	MU-WDS	MU-WDS
SiO_2	40.76	34.08	33.52	33.96	34.28	33.82	34.09	34.10	-	-	-	-	-
TiO_2	0.05	1.11	1.08	1.06	1.09	1.08	1.08	1.04	-	-	-	-	-
Al_2O_3	34.47	17.45	17.34	16.89	17.22	17.17	17.63	17.14	-	-	-	-	-
Cr_2O_3	0.12	0.20	0.24	0.16	0.18	0.19	0.15	0.14	-	-	-	-	-
FeO	2.31	21.51	20.75	20.35	21.22	20.91	21.16	20.63	11.19	11.69	6.67	11.36	11.48
MnO	0.02	0.10	0.07	0.09	0.08	0.11	0.09	0.11	1.50	1.30	1.08	1.49	1.33
NiO	BDL	BDL	BDL	BDL	BDL	BDL	BDL	BDL	-	-	-	-	-
MgO	1.04	9.87	9.88	10.14	10.04	10.06	9.82	9.99	13.22	13.14	7.37	13.20	13.36
CaO	0.04	0.05	0.06	0.20	0.10	0.15	0.26	0.30	18.94	18.78	26.01	18.65	18.84
BaO	6.14	2.12	2.31	2.05	2.03	1.91	2.13	1.87	BDL	BDL	BDL	BDL	BDL
SrO	-	-	-	-	-	-	-	-	BDL	0.04	0.03	0.03	0.05
Na_2O	0.63	0.22	0.17	0.23	0.18	0.12	0.15	0.17	-	-	-	-	-
K_2O	8.52	8.87	8.81	7.90	8.75	8.64	8.61	9.05	-	-	-	-	-
Cl	BDL	0.36	0.34	0.35	0.38	0.34	0.35	0.36	-	-	-	-	-
F	BDL	0.08	0.06	0.08	0.12	0.08	BDL	0.09	-	-	-	-	-
SO_2	BDL	BDL	BDL	BDL	BDL	BDL	BDL	BDL	BDL	BDL	BDL	BDL	BDL
Total	94.10	96.02	94.63	93.46	95.67	94.58	95.52	94.99					

	B dol-6	B dol-7	B dol-8	B cal-1*	A phlog-1	A dol-1	A dol-2	A dol-3	A dol-4	C phlog-1	C hyal-1	C hyal-2
	MU-WDS	MU-WDS	MU-WDS	MU-WDS	UW-EDS	UW-EDS	UW-EDS	UW-EDS	UW-EDS	UW-EDS	UW-EDS	UW-EDS
SiO_2	-	-	-	-	37.02	0.17	0.04	BDL	BDL	36.7	56.96	54.11
TiO_2	-	-	-	-	1.01	-	-	-	-	1.52	BDL	BDL
Al_2O_3	-	-	-	-	18.55	BDL	BDL	0.13	0.01	17.14	20.58	21.26
Cr_2O_3	-	-	-	-	-	-	-	-	-	-	-	-
FeO	11.32	11.00	3.57	1.19	20.93	21.28	19.84	25.60	21.07	23.97	0.40	0.51
MnO	1.28	1.31	1.09	0.44	0.15	2.14	2.28	2.58	2.42	0.08	0.07	BDL
NiO	-	-	-	-	-	-	-	-	-	-	-	-
MgO	13.53	12.85	2.08	0.64	10.19	24.38	25.50	21.43	26.84	8.78	0.03	0.06
CaO	18.73	18.46	31.95	22.66	0.10	52.03	52.34	50.20	49.66	0.14	0.14	0.18
BaO	BDL	BDL	BDL	BDL	2.61	BDL	BDL	BDL	BDL	2.10	11.15	13.49
SrO	0.01	BDL	0.01	BDL	-	-	-	-	-	-	-	-
Na_2O	-	-	-	-	0.19	-	-	-	-	BDL	BDL	0.98
K_2O	-	-	-	-	8.87	-	-	-	-	9.26	10.67	9.37
Cl	-	-	-	-	0.36	-	-	-	-	0.31	-	-
F	-	-	-	BDL	BDL	BDL	BDL	BDL	BDL	BDL	BDL	BDL
SO_2	BDL	BDL	BDL	BDL	-	-	-	-	-	-	-	-
Total					99.98					100.00	100.00	99.96

G12/93 locality 'A' 0.8 mm wide laser ablation ICPMS traverse Refer to Extended Data Figure 4 for location of segments												Other analyses at stromatolite site	
segment #	1	2	3	4	5	6	7	8	9	10	11	G11/63	G11/72
	sediment below	sediment below	sediment below	sediment below	sediment below	sediment below	sediment below	within stromat.	within stromat.	within stromat.	sediment above	dolostone	breccia
length (mm)	5.5	0.83	1.07	1.1	1.23	0.4	6.29	6.57	9	4	8		
oxides wt%													
SiO_2	18.70	33.75	14.56	36.86	14.22	72.58	15.35	30.92	38.03	16.12	38.25		
Al_2O_3	3.68	8.15	4.97	4.76	1.15	2.77	1.77	1.15	1.21	0.74	4.51		
$FeCO_3$	9.74	7.73	10.76	8.60	11.39	2.98	11.66	9.74	9.31	13.11	8.31		
$MgCO_3$	13.57	7.48	14.43	10.09	17.33	3.98	17.92	15.39	12.07	17.81	9.56		
$CaCO_3$	49.33	23.37	48.63	28.18	58.92	14.56	56.90	44.81	38.01	58.19	29.22		
Total	85.27	72.74	82.59	79.90	91.63	93.88	91.95	92.27	89.32	92.86	81.54		
ppm													
Li	12.6	29.4	18.3	22.1	4.8	4.3	6.0	3.7	3.1	2.9	14.4		
P	25.9	8.2	5.2	8.0	806.6	560.6	21.2	72.5	85.9	104.2	17.9		
Ti	568	1330	781	953	211	120	252	142	116	104	619		
V	44.5	101.7	61.3	62.5	14.6	28.4	21.6	12.5	12.2	8.8	52.6		
Cr	323	917	575	627	124	126	147	40	26	81	437	210	140
Co	15.6	19.2	18.5	17.5	14.9	4.0	14.5	10.9	9.2	12.6	11.4		
Ni	47.1	91.5	63.1	72.3	32.0	12.3	33.3	23.6	19.0	24.1	37.3		
Zn	35.8	48.0	42.0	42.8	33.3	12.8	32.5	26.1	23.1	28.6	31.0		
Ga	3.02	7.05	4.17	4.13	0.99	2.41	1.48	0.89	0.92	0.60	3.71		
Rb	31.9	75.8	44.1	53.3	12.1	12.2	14.4	8.8	7.4	6.5	37.1	22.4	17
Sr	46.4	29.5	47.0	27.0	53.5	16.0	52.1	41.2	34.8	53.5	30.9	63.4	17.5
Y	8.27	10.82	8.61	4.59	8.16	4.88	7.05	5.09	4.51	9.52	8.31	6.6	8
Zr	10.4	28.9	11.0	7.0	3.6	8.4	3.8	3.8	5.2	6.0	16.5	9	14
Nb	0.29	0.68	0.41	0.46	0.10	0.13	0.14	0.09	0.08	0.06	0.37	0.5	0.6
Ba	1843	3862	2453	2069	525	1661	942	597	886	409	2350	1295	9640
La	2.72	8.47	2.93	1.59	1.09	1.67	2.21	1.24	0.94	2.60	2.58	2.2	2.4
Ce	4.49	13.80	4.76	2.76	1.78	2.80	3.73	2.18	1.71	4.37	4.22	3.4	3.5
Pr	0.54	1.63	0.57	0.33	0.22	0.34	0.46	0.28	0.22	0.53	0.50	0.41	0.39
Nd	2.35	7.03	2.44	1.41	1.04	1.34	2.09	1.26	1.03	2.35	2.07	1.6	1.4
Sm	0.61	1.60	0.63	0.38	0.34	0.36	0.58	0.37	0.32	0.64	0.51	0.4	0.29
Eu	0.34	0.66	0.33	0.22	0.25	0.30	0.33	0.25	0.21	0.34	0.26	0.46	0.15
Gd	0.83	1.71	0.84	0.51	0.65	0.50	0.80	0.56	0.48	0.94	0.67	0.66	0.67
Tb	0.14	0.24	0.15	0.09	0.13	0.09	0.14	0.10	0.09	0.17	0.12	0.11	0.12
Dy	1.00	1.47	1.01	0.57	0.95	0.62	0.91	0.67	0.60	1.15	0.90	0.66	0.73
Ho	0.23	0.30	0.24	0.13	0.23	0.14	0.21	0.16	0.14	0.27	0.23	0.17	0.19
Er	0.72	0.87	0.74	0.39	0.68	0.39	0.60	0.46	0.41	0.82	0.73	0.46	0.53
Tm	0.11	0.13	0.11	0.06	0.10	0.06	0.09	0.07	0.06	0.12	0.12	0.07	0.08
Yb	0.73	0.89	0.77	0.41	0.64	0.39	0.59	0.44	0.39	0.83	0.82	0.46	0.49
Lu	0.12	0.12	0.07	0.10	0.07	0.10	0.08	0.07	0.07	0.13	0.13	0.09	0.08
Hf	0.33	0.36	0.24	0.13	0.33	0.13	0.14	0.00	0.17	0.13	0.54	0.3	0.5
Pb	2.26	2.25	1.83	2.18	1.57	2.10	2.02	18.62	1.96	2.28	2.29		
Th	0.22	1.01	0.22	0.11	0.10	0.23	0.11	0.00	0.08	0.18	0.27	0.13	0.25
U	0.07	0.11	0.06	0.04	0.07	0.05	0.05	0.01	0.06	0.09	0.10	0.06	0.1

Extended Data Table 3. Carbon and Oxygen isotopic analysis of a site 'A' stromatolite

	$\delta^{13}C_{VPDB}$	$\delta^{18}O_{VSMOW}$raw	$\delta^{18}O_{VSMOW}$corr	$\delta^{18}O_{VPDB}$approx*
A-a	1.41	19.38	18.46	-12.07
	1.31	19.39	18.47	-12.06
A-b	1.44	19.37	18.45	-12.08
	1.48	19.26	18.34	-12.19
	1.47	19.33	18.41	-12.12
A-c	1.41	19.34	18.42	-12.11
	1.35	19.20	18.28	-12.25
	1.46	19.25	18.33	-12.20
A-d	1.20	19.23	18.31	-12.22
	1.22	19.17	18.25	-12.28
A-e	1.30	19.31	18.39	-12.14
	1.35	19.25	18.33	-12.20

* The VPDB $\delta^{18}O$ scale strictly only applies to calcite, not to other carbonates.
Accordingly, the data column labelled '$\delta^{18}O_{VPDB}$approx' refers to the conversion from the corrected $\delta^{18}O_{VSMOW}$ values using $\delta^{18}O_{VPDB}=0.97002(\delta^{18}O_{VSMOW})-29.98$.
See Extended Data Figure 6 for location of analyses
The replicate analyses refer to separate CO_2 extractions of powdered sample